RSC Advances

ROYAL SOCIETY OF CHEMISTRY

www.rsc.org/advances

Table of Contents

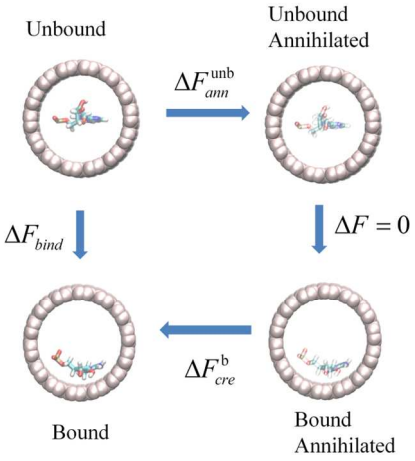

The binding free energy is in the order A-zigzag SWNT (24,0) > T-zigzag SWNT (24,0) > A-armchair SWNT (14,14) > T-armchair SWNT (14,14).

On the loading mechanism of ssDNA into carbon nanotubes

Jia-Wei Shen,[a] Ting Tang,[a] Xiao-Hong Wei,[a] Wei Zheng,[a] Tian-Yang Sun,[b] Zhisen Zhang,[c] Lijun Liang,*[,bd] Qi Wang*[,b]

[a]*School of Medicine, Hangzhou Normal University, Hangzhou 310016, People's Republic of China.*

[b]*Department of Chemistry and Soft Matter Research Center, Zhejiang University, Hangzhou, 310027, People's Republic of China*

[c]*Research Institute for Soft Matter and Biomimetics, Department of Physics, Xiamen University, Xiamen, 361005, People's Republic of China*

[d]*Department of Polymer Science and Engineering, Zhejiang University, Hangzhou 310027, People's Republic of China.*

*Corresponding authors.

Fax: +86-571-87951895

E-mail addresses: michael.lijunl@gmail.com (L. Liang); qiwang@zju.edu.cn (Q. Wang)

Abstract

Understanding of the mechanism and dynamics of DNA loading into carbon nanotubes (CNTs) is very important for the promising applications of CNTs in DNA sequencing, drug delivery and gene delivery systems etc. In this work, the loading mechanism and dynamics of different ssDNA oligomers into single-walled carbon nanotubes (SWNTs) was investigated through molecular dynamics simulations, steered molecular dynamics simulation and binding free energy calculations. Our simulation results showed that the loading of different ssDNA oligomers into the zigzag SWNT is much easier than the armchair SWNT does. Confined in both zigzag and armchair type SWNTs, ssDNA oligomers have helical structure and their bases adapt the orientation that parallel to the interior wall. From detailed analysis of the interaction energy, potential of mean force (PMF) of unloading process and nucleotide binding free energy, our results show that the chirality of SWNTs has large effect on the binding strength of nucleotides, and hence affect the loading dynamics of ssDNA into SWNTs.

Keywords: *Carbon nanotubes; ssDNA oligomers; Drug delivery; Loading dynamics; Molecular dynamics; Thermodynamic integration*

1. Introduction

The properties and applications of the organic-inorganic nano-material with the size varied from about one nanometer to several hundred nanometers have attracted many researchers' focus.[1-3] It has great expectations on its potential applications in nanotechnology and biotechnology,[4,5] and presented new opportunities for biomedical research such as drug delivery, gene delivery etc. In particular, carbon nanotubes (CNTs) rolled seamless from the single graphene sheets exhibited unique physical, mechanical and chemical properties which has attracted tremendous interests in the past decade.[6-8] As a type of organic-inorganic nano-complex, the biomolecule-CNTs complex has aroused huge attentions for many years due to its board applications on CNTs solubilization,[9,10] biosensors,[11,12] drug delivery device[13,14] and gene delivery.[15,16] In particular, the major advantages of targeted drug delivery by CNTs are that it enables a stronger drug to be used at a smaller dosage, and it has fewer side effects than current delivery methods such as chemotherapy, which is limited by the inadequate and nonspecific delivery of therapeutic concentrations to target the tumor tissue. CNTs offer the perfect isolated environment for the drug until it reaches the target site, both from degradation and reaction with healthy cells. Especially, CNTs could be inserted into the cell membrane with the function as a channel, and shows excellent transport properties to transport ions, water and DNA etc.[17] Their ability to be functionalized and visualized in biological environments using simple fluorescence microscopy has further enhanced their application in nanomedical field.[18]

To realize these applications, the properties including the details of interaction mechanism and the fundamental molecular properties related to biomolecule-CNTs in the biological setting should be well understood. Moreover, the dynamics and the mechanism of biomolecules loading into the CNTs is also very important for its real use in drug delivery system and gene delivery device, or being a biomimetic CNTs in cell membrane. These properties have been explored by experimental groups in recent years.[19-21] Dai *et al*. pointed out that the peptide and DNA molecules could be taken by CNTs, and it could be used as drug delivery system.[20] By using atomic force microscope (AFM), Noy *et al*. found that DNA molecule could be pulled out from the CNTs with a constant force.[21] To understand the mechanism of DNA encapsulation into the CNTs from the molecular level, many molecular dynamics simulation have been performed.[22-24] In addition, many works from our group[25] and other groups[26-28] found that the water molecules have effects on the loading of DNA into CNTs. Pasquali *et al* observed the dynamics of single-walled carbon nanotubes (SWNTs) in aqueous suspension by fluorescence video microscopy.[26] Kolesnikov *et al*. investigated the dynamics of water molecules in CNTs through neutron scattering techniques.[27] Hummer and co-workers[28] reported a one-dimensionally ordered chain of water molecules

to transport through the hydrophobic SWNTs. Recently, the mechanism of spontaneous insertion of peptide into SWNTs has been investigated in our group.[29-31] In these works, the diameters and chirality of SWNTs was considered as key factors to affect the dynamics of peptides.

Although there are some progresses on the field of encapsulation of biomolecules into CNTs, the loading mechanism and dynamics of peptide, protein and DNA into the CNTs with different structure and chirality is rarely studies and remains obscure, which may limit the real application of CNTs as drug and gene delivery system. In this study, we investigate the loading mechanism of different type of ssDNA oligomers into SWNTs as well as the effect of SWNTs chirality on the loading of ssDNA oligomers by MD simulations. Different chirality including zigzag and armchair type of SWNTs were used to explore the effects of the geometry and topology of SWNTs on the spontaneous loading of ssDNA and binding on the interior wall of SWNTs.

2. Simulation methods

In this study, all MD simulations were performed by program NAMD.[32] The CHARMM27 force field[33] was used for ssDNA and TIP3P[34] model was used for water molecules. The parameters of carbon nanotubes were taken from the work of Walther et al.[35] The parameters of Lennard-Jones potential for the cross interactions between non-bonded atoms ($e.g.$, SWNT-ssDNA) were obtained from the Lorentz-Berthelot combination rules as in our previous studies.[36,37] Two ssDNA consisting 8 homogeneous adenines and thymines were used in these simulations for the consideration of investigating the effect of adenosine and purine on the loading mechanism of ssDNA into SWNTs. The name of poly$(A)_8$ and poly$(T)_8$ were adapted to refer to these two types of ssDNA for simplicity in the following section of this paper. SWNTs with different chirality were individually used in these simulations, namely, zigzag (24,0) and armchair (14,14) SWNTs, and they have similar diameters around 19.0 and 18.8 Å. The lengths of these SWNTs are 52.5 and 54.0 Å, which are long enough to encapsulate the ssDNA oligomers and eliminate the size effect. All atoms including hydrogen atoms were described explicitly in all simulations. The switching function of non-bonded van der Waals force started at a distance of 10 Å and reached zero at 12 Å. The Particle mesh Ewald (PME) summation[38] was used to calculate the long-ranged electrostatic interactions, with a cutoff distance of 12 Å for the separation of the direct and reciprocal space. The time step of the simulation was 2 fs, and periodic boundary conditions (PBC) were applied in all MD simulations. During all MD simulations, the Langevin thermostat was used to control the constant temperature at 310 K and Langevin piston Nose-Hoover method was used to control the pressure at 101.3 kPa. All MD simulations were carried out in NPT ensemble with velocity Verlet numerical integrator.

Simulations were firstly performed by energy minimization and then 5 ns pre-equilibration of the ssDNA (both poly(A)$_8$ and poly(T)$_8$) in TIP3P water was carried out. Then one end of the pre-equilibrated ssDNA was putted around 4 Å close to one end of uncapped SWNT, with the central axis of both ssDNA and SWNT were aligned in the same line. The central axis of both ssDNA and SWNTs were set to parallel to the *z*-direction of the simulation box, thus the cross sections of the SWNTs were in the *x*-*y* plane. There are four combination of these ssDNA-SWNT complexes, namely, A8 in zigzag SWNT (24,0), A8 in armchair SWNT (14,14), T8 in zigzag SWNT (24,0) and T8 in armchair SWNT (14,14), respectively. The names of A8@SWNT (24,0), A8@SWNT (14,14), T8@SWNT (24,0) and T8@SWNT (14,14) were used to refer to these different complexes in the following section of this paper for simplicity. These complexes were solvated in TIP3P water, and the number of water molecules contained in the simulation boxes is from 6386 to 6747, due to the different box sizes of the systems. The box size of four systems is around 42.7 × 42.7 × 129.5 Å^3. All carbon atoms of SWNT were fixed and ssDNA were kept relaxed during the loading process in all simulations. Fig. 1 shows the initial configuration of a pre-equilibrated ssDNA and SWNTs system (water molecules are omitted for clarity) before system minimization and MD simulation. Here only A8@SWNT (24,0) and T8@SWNT (24,0) systems were displayed, however, the initial configurations of other two systems are similar.

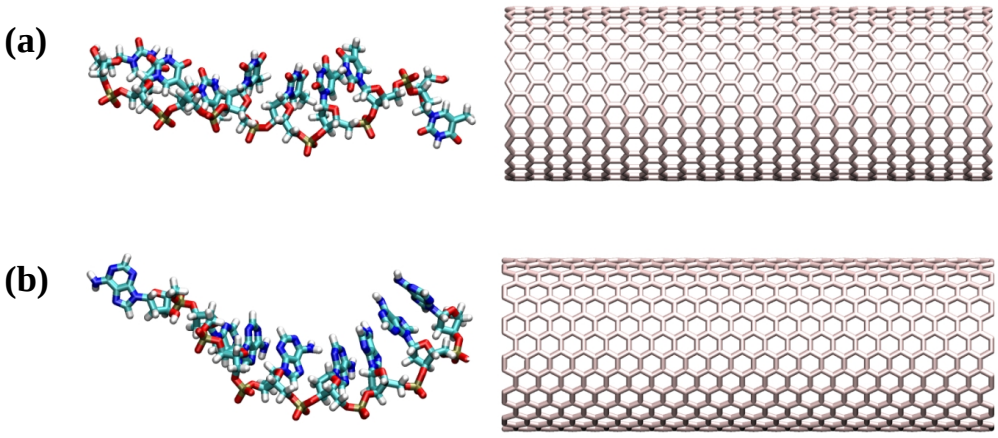

Fig. 1 The snapshots of initial orientation of ssDNA oligomers to SWNTs in our simulations. (a) A8@SWNT (24, 0) and (b) T8@SWNT (14,14). The central axis of both ssDNA and SWNTs were set to parallel to the *z*-direction of the simulation box, and the cross sections of the SWNTs were in the *x*-*y* plane. Both ssDNA oligomers and SWNTs are represented by licorice model. Water molecules are omitted for the clarity. Oxygen is rendered in red, nitrogen in blue, phosphor in yellow, carbon in the ssDNA is rendered in cyan, and carbon in SWNTs is rendered in silver.

These systems (containing SWNT, ssDNA oligomer and water molecules) were performed 10000 steps energy minimization at first, then 40 ns MD simulation were carried out to study the loading mechanism and dynamics of ssDNA into SWNTs with different chirality (for the system of A8@SWNT (24,0), only 20 ns MD simulation was carried out and it will be discussed with more details in the following section). The time-dependent interaction, $E_{int}(t)$ for all the systems in MD simulations were used to qualitatively understand the interaction strength between SWNTs and ssDNA, and it was defined as follows:

$$E_{int}(t) = E_{SWNT+ssDNA}(t) - E_{SWNT}(t) - E_{ssDNA}(t) \quad (1)$$

In equation (1), $E_{int}(t)$ stands for the total interaction energy between ssDNA and the SWNT surfaces at time t during the MD simulation, and $E_{SWNT+ssDNA}(t)$, $E_{SWNT}(t)$, $E_{ssDNA}(t)$ are the total potential energy of the SWNT-ssDNA complex, the potential energy of SWNT and that of ssDNA at time t during MD simulations, respectively. This method has been successfully applied to investigate the adsorption mechanism of peptide and proteins on exterior and interior wall of carbon nanotubes.[29, 36,37]

To better understand the thermodynamics of ssDNA loading process, for all systems containing CNTs and ssDNA, steered molecular dynamics (SMD) simulations were performed to calculate the potential of mean force (PMF) during the ssDNA encapsulation process based on Jarzynski's equality. The difference of free energy between two states (totally encapsulated state and starting state) is connected to the work W done on the system through equation 2,

$$e^{-\beta \Delta G} = \langle e^{-\beta W} \rangle \quad (2)$$

where $\beta = 1/k_B T$ is the inverse temperature and k_B is the Boltzmann constant.

After the encapsulation of ssDNA into SWNTs, 10 ns more MD simulation was performed to equilibrate all systems. During these simulations, the center of the ssDNA was constrained in the same position of the center of mass of SWNT in z direction (along the central axis). Then the configurations of ssDNA@SWNT complex in last frame in these MD simulations were used as the initial structure for the constant velocity pulling to obtain the PMF profile. An external force was applied to the center of mass of ssDNA and ssDNA was pulled out along the z direction. The pulling distance was set to be 7.0 nm to make sure that ssDNA could be pulled out from SWNT. The spring constant k was set as 41.84 kJ/mol·Å^2, and the pulling velocity was fixed at 3.5 Å/ns. For system T8@SWNT (14, 14), poly(A)$_8$ was firstly pulled into the SWNT until the center of mass of poly(A)$_8$ and SWNT overlap in z direction. Then same treatment as other three systems was applied for this system. To obtain the PMF profile of ssDNA (poly(A)$_8$ and poly(T)$_8$) leaving zigzag or armchair SWNT, SMD simulations of each system were

repeated 12 times, and the free energy is calculated from the average of the work done in these 12 simulations according to equation 2.

Thermodynamic integration (TI) method[39] was used for the calculation of binding free energy of single nucleotide on the interior wall of SWNTs with different chirality. These systems consisted of a single nucleotide with a SWNT (zigzag or armchair type) in aqueous solution in a 39.5 × 39.5 × 104.0 $Å^3$ cell box. The force field and simulation parameters have been described above. The systems were equilibrated for 20 ns before free energy perturbation calculations. The binding free energy could be calculated by annihilating or creating a nucleotide in the unbound and bound states, respectively. The difference in the free-energy was calculated in two-step process. Firstly, electrostatic interaction was turn off/on by annihilating/creating atomic charges with λ values varied from 0.0, 0.3, 0.6, 0.9, and 1.0. Secondly, vdW interaction was annihilated/created by using λ values of 0.0, 0.1, 0.2, 0.3, 0.4, 0.5, 0.6, 0.7, 0.8, 0.9 and 1.0. To prevents overlapping particles from making the simulation unstable, soft-core Lennard-Jones potentials were employed with the efficient parameter α = 0.5. Thus, the contribution of electrostatic (ΔF_{ele}) and vdW (ΔF_{vdW}) to ΔF_{bind} was calculated. At each λ value, 10 ns MD were performed to ensure the sampling is adequate by using a 2 fs timestep, and the ensemble average $\langle \partial H / \partial l \rangle$ was extracted in the last 5 ns trajectory. To estimate the error of contribution from electrostatic and vdW to binding free energy, all processes were repeated in an opposite direction in thermodynamic cycle.

3. Results and discussion

Except system T8@SWNT(14,14), all other systems have been observed the spontaneous and total insertion into the cavity of the SWNTs in MD simulation. Fig. 2 shows the snapshots of the ssDNA oligomers encapsulated into the zigzag (24,0) and armchair (14,14) SWNTs after MD simulations. For system A8@SWNT (24,0), the ssDNA oligomers gradually inserted into the interior space of the SWNTs during first 10 ns. After 10 ns, poly(A) was totally loaded into the cavity of SWNT and confined with helical structure. During this period, the movement of $poly(A)_8$ inside SWNT (24,0) was only slightly fluctuated. This could be validated by the trajectory and the root mean square deviation (RMSD) of $poly(A)_8$ during the loading process, as displayed in Fig. 3(a). The RMSD value of $poly(A)_8$ fluctuate mildly after total encapsulation. The helical structure of biomolecules in SWNTs could also be found in our previous work.[30] Moreover, most of the bases of $poly(A)_8$ adapt the orientation that lie flat on the interior wall. This indicates very strong π–π stacking interaction between adenine and wall, and similar phenomena have been observed in other biomolecule-SWNT complexes.[36,37,40] The details of the deduction will be discussed in rest part of this paper.

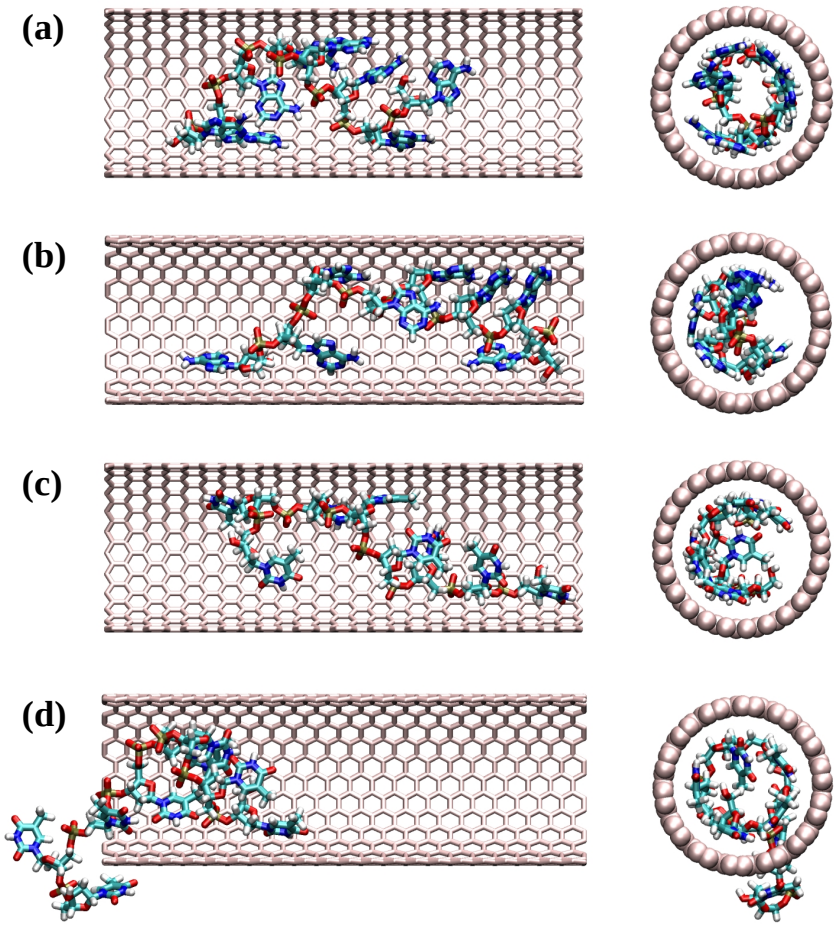

Fig. 2 The snapshots of the side view and top view of final state of ssDNA oligomers encapsulated in zigzag (24,0) and armchair (14,14) SWNTs. (a) A8 in zigzag SWNT (24,0), (b) A8 in armchair SWNT (14,14), (c) T8 in zigzag SWNT (24,0) and (d) T8 in armchair SWNT (14,14). ssDNA are represented by licorice model. SWNTs are represented by licorice model in side view and by VDW model in top view. Water molecules are omitted for the clarity. For side view of all snapshots, half of the SWNTs are omitted to give the best view of ssDNA oligomer adsorbed on the interior wall of SWNTs.

Since the loading dynamics of poly$(A)_8$ in SWNT (24,0) observed in MD simulation is fast compare with other ssDNA oligomers, the simulation was carried out for totally 20 ns. However, for system A8@SWNT(14,14) and T8@SWNT(24,0), the total insertion of ssDNA oligomers were observed within 40 ns, validated by both simulation trajectory as well as the normalized distance of center-of-mass (COM) of ssDNA to the geometric center of the SWNTs (in *z* direction, parallel to the central axis of SWNTs)

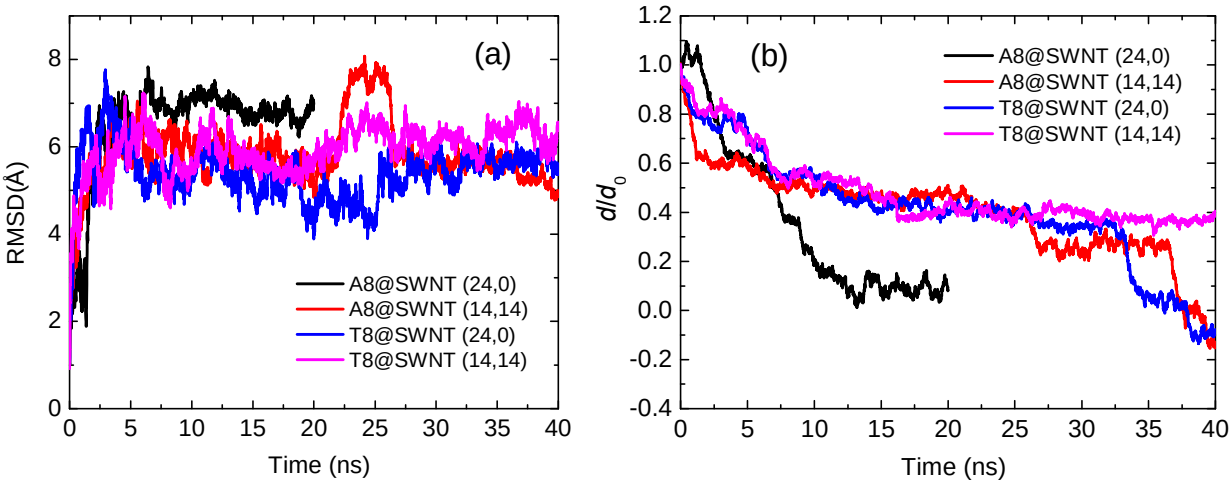

Fig. 3 (a) Root mean square deviation (RMSD) of ssDNA during the loading process into the cavity of SWNTs. (b) The normalized distance of center-of-mass (COM) of ssDNA to the geometric center of the SWNTs in *z* direction (parallel to the central axis of SWNT) during the loading process into the cavity of SWNTs. Here non-hydrogen atoms in ssDNA were selected to calculate the RMSD.

during the loading process, d/d_0, as shown in Fig. 3(b). Herein, the variable d represents the distance of COM of ssDNA to the geometric center of SWNTs in *z* direction with respect to the simulation time, and d_0 is the initial value of d before MD runs. The value of d/d_0 approached 0 (which mean the overlap of the COM of ssDNA and SWNTs) around 35 ns for both A8@SWNT(14,14) and T8@SWNT(24,0) systems. During the loading process in these two systems, both poly(A)$_8$ and poly(T)$_8$ have helical structure inside SWNTs with majority of their bases lie flat on the interior wall, as displayed in Fig. 2(b) and 2(c). The similarity of the ssDNA conformation and binding of the base indicates that the ssDNA would prefer to have the helical structure to increase the contact area between their bases and wall in the interior confined space of SWNTs. In this way, the penalty of the conformational change could be compensated by the maximized interaction between bases and wall. The helical structures of small molecules inside SWNTs have also been found in both theoretical and experimental work due to the chirality of SWNTs.[25,41] Starting from 20 ns, poly(T)$_8$ got stuck at one open end of SWNT (14,14) with 3 thymine still located in the exterior space of SWNT (14,14) , and the value of d/d_0 only slightly fluctuated until 40 ns, as shown in Fig. 3(b). The result may indicate insufficient driving force or larger energy barrier of system T8@SWNT (14,14) that lead to slow loading dynamics comparing with other systems. Extension of simulation time to 60 ns still had the problem of getting stuck for poly(T)$_8$ in SWNT (14,14), and it is difficult to judge the reasonable time for total insertion of poly(T)$_8$, therefore, we didn't further extend the simulation time, and we use the first 40 ns simulation trajectory for analysis and comparison. However, the part of poly(T)$_8$

that already inserted into the cavity of SWNTs has similar helical structure and orientation of the bases as the oligonucleotides in other three systems. In short summary, the loading time for four system observed in our MD simulation is roughly in the order A8@SWNT (24,0) < T8@SWNT (24,0) ≈ A8@SWNT (14,14) < T8@SWNT (14,14). However, one has to notice that this result is only observed with specific starting configuration and position of ssDNA. Only further loading free energy and nucleotide binding free energy calculation could well explain the loading mechanism and dynamics of ssDNA.

To understand the loading mechanism and the reason behind the results mentioned above, we calculated the interaction energy between different type of ssDNA oligomers and SWNTs as well as interaction energy between all bases of these oligomers and SWNTs during the simulation time, as shown in Fig. 4. Not surprisingly, poly$(A)_8$ possesses the highest interaction energy around -368.1 kJ/mol with zigzag SWNT (24,0), while for A8@SWNT (14,14), T8@SWNT (24,0) and T8@SWNT (14,14) systems, the interaction energy between ssDNA oligomers and SWNTs is -346.2, -332.0 and -300.4 kJ/mol, respectively. Meanwhile, the interaction energy between all bases in ssDNA oligomers and SWNTs in A8@SWNT (24,0), A8@SWNT (14,14), T8@SWNT (24,0) and T8@SWNT (14,14) systems are -213.8, -202.3, -173.3 and -152.6 kJ/mol, respectively. It clearly shows that the binding of the bases to interior wall of SWNTs contributes the majority of interaction strength between ssDNA oligomers and SWNTs, and this is probably the driving force of the encapsulation of ssDNA into SWNTs. Therefore, the interaction energy between ssDNA oligomers and SWNTs has the similar trend with the interaction energy between bases and SWNTs, as shown in Fig. 4. More interestingly, both of them exhibit stepwise decrease, and it is more obvious for interaction between bases and SWNTs. Similar phenomena have been found in peptide-SWNT complex systems in our previous papers.[29,36] In the cases of this study, during the loading of ssDNA oligomer into the cavity of SWNTs, the binding of the single-bases to the interior wall stabilize the ssDNA-SWNT complex and gradually drive the ssDNA oligomers to the inner space of SWNTs. Thus the stepwise increase of the interaction strength mainly attribute to the single-base binding to the wall during the loading process. On the other hand, take A8@SWNT (24,0) and T8@SWNT (24,0) systems for example, the interaction strength between bases of poly$(A)_8$ and SWNT (24,0) are 36.1 kJ/mol stronger than that between bases of poly$(T)_8$ and SWNT(24, 0). The reason is that adenine has larger conjugated aromatic rings than thymine, and it has stronger π–π stacking interaction.

In a recent paper of our group,[30] we found that in aqueous solution, the armchair SWNT (14,14) encapsulated the peptide much easier than the zigzag SWNT (24,0) did. However, in this study for ssDNA loading, the situation is opposite. Take A8@SWNT (24,0) and A8@SWNT (14,14) systems for example, poly$(A)_8$ totally inserted into the cavity of SWNT (24,0) within 10 ns, while the whole poly$(A)_8$ inserted into SWNT (14,14) after 35 ns, as displayed in Fig. 3(b). This is not difficult to understand since

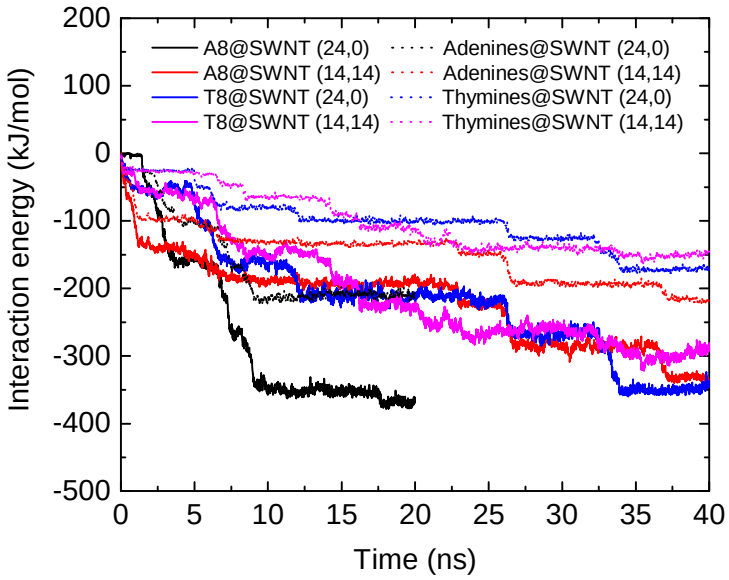

Fig. 4 The interaction energy between different type of ssDNA oligomers and SWNTs (solid line) as well as interaction energy between all bases of these oligomers and SWNTs (dotted line) with respect to the simulation time.

the interaction strength between poly$(A)_8$ and SWNT (24,0) is 21.9 kJ/mol stronger than that between poly$(A)_8$ and SWNT (14,14). Meanwhile, the interaction strength between bases of poly$(A)_8$ and SWNT (24,0) is 11.5 kJ/mol stronger than that between bases of poly$(A)_8$ and SWNT (14,14). For A8@SWNT (24,0) and A8@SWNT (14,14) systems, similar result could be found. Therefore, the difference of interaction energy between ssDNA and SWNTs in these systems is mainly attributed to the binding strength of bases to SWNTs wall. Since the binding of adenine and thymine to SWNT (24,0) is much stronger than that of SWNT (14,14), it lead to stronger interaction between ssDNA oligomers and SWNT (24,0) during the loading process. This could also be validated by the normalized probability distribution of all bases around the wall of SWNTs, shown in Fig. 5(a). The maximum distribution of all bases is from 0.36 to 0.37 nm away from the wall of SWNTs, and this distance is the typical distance between two conjugated systems with π–π stacking interactions.[42] One could also found that adenine have larger distribution around wall of zigzag SWNT (24,0) comparing with armchair SWNT (14,14) (black and red line). As the diameter of these two SWNTs in our simulation is very close (see section "Simulation Method"), the difference of distribution should attribute to the effect of chirality of SWNTs on the binding of bases, and this effect could affect the confinement of ssDNA oligomers inside the cavity of SWNTs. This effect may origin from the fit of the helical arrangement of bases of ssDNA and helical arrangement of the hexagonal ring in SWNT with different chirality. Similarly, thymine have less

distribution around wall of armchair SWNT (14,14) comparing with zigzag SWNT (24,0), which also indicates weaker affinity of thymine to armchair SWNT (14,14). This may be the reason that T8@SWNT (14,14) system has the slowest loading dynamics of ssDNA oligomers among all the systems in this study. In Fig. 5(b), we also plotted the normalized distribution of water molecules around interior wall of SWNTs for all systems. It shows that for both zigzag SWNT (24,0) and armchair SWNT (14,14) it has two solvation layers around interior wall. For both SWNTs with different chiralities, the solvation layers roughly located at 0.35 and 0.63 nm away from the wall. As the highest distribution of bases is around 0.36 nm, it indicates that the bases have the competition with water for the binding site to the interior wall of SWNTs. For different type of nucleotides in the same type of SWNTs, the water structure in the first solvation layer is less affected. However, the distribution of water in the first solvation layer for both bases in zigzag SWNT (24,0) is lower than that in armchair SWNT (14,14).

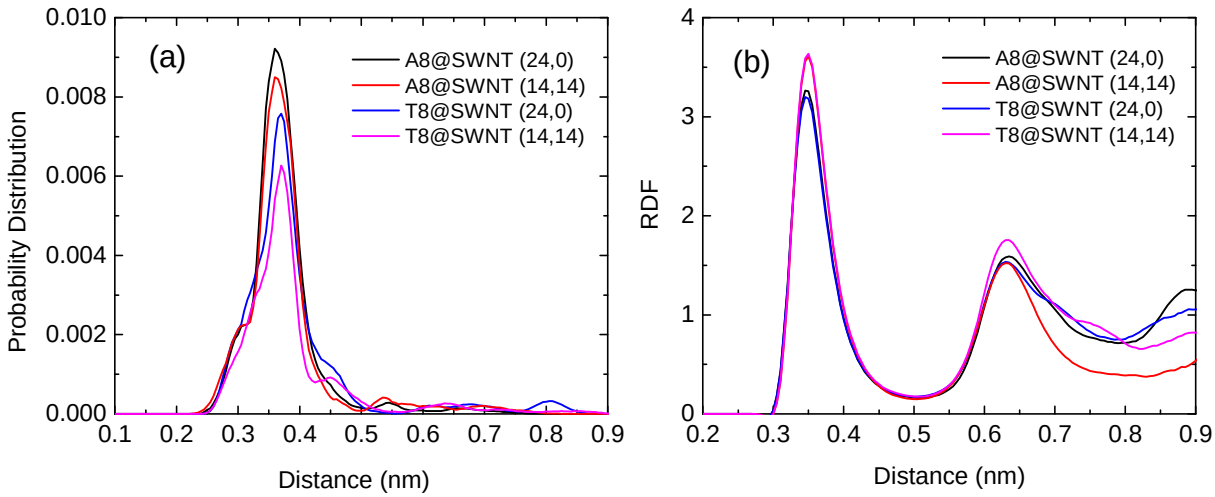

Fig. 5 (a) Normalized probability distribution of all bases around the wall of SWNTs and (b) normalized radial distribution function (RDF) of water molecules around interior wall of SWNTs in four systems in this study.

Fig. 6 shows the PMF profile for all systems on the basis of SMD simulations. The starting structure during the pulling process was set as the zero point of free energy. The free energy different for system A8@SWNT (24,0), A8@SWNT (14,14), T8@SWNT (24,0) and T8@SWNT (14,14) are -235.59, -217.52, -204.83 and -199.97 kJ/mol, respectively. In general these free energy profiles are smooth and there are no obvious energy barrier was found. Since free energy is a state function, it is obvious that the loading process of poly(A)$_8$ into zigzag SWNT (24,0) possess the highest free energy change, this is probably the reason that it has the lowest loading time. On the other hand, the free energy change during

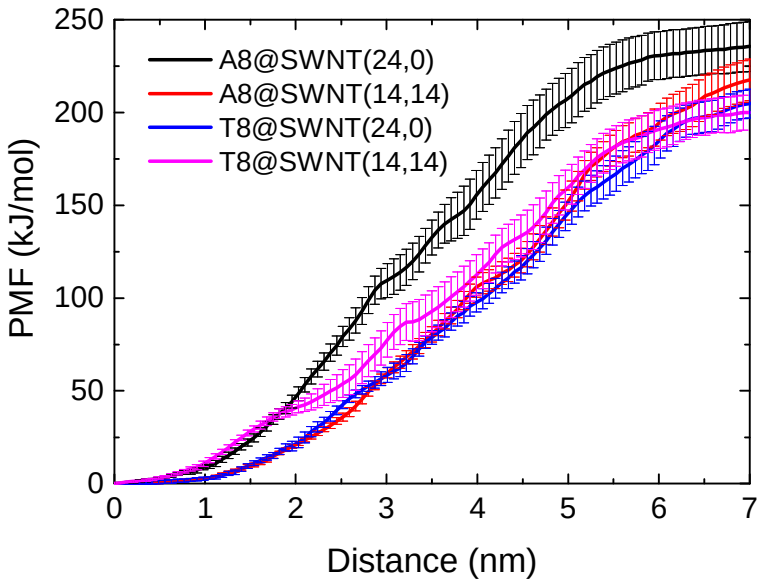

Fig. 6 The potential of mean force (PMF) profile for all systems during the pulling process.

the loading of poly(T)$_8$ into armchair SWNT (14,14) is lowest and this is probably the reason that it has the lowest loading dynamics in our MD simulation. The free energy calculation by SMD simulation of pulling ssDNA out of SWNT could generally explain the order of loading dynamics we observed in MD simulation.

Although free energy calculation of ssDNA encapsulation could give general description of ssDNA loading dynamics, it is difficult to have sufficient sampling of large conformational space of ssDNA during the loading process and it is also hard to get very accurate free energy values. To describe the effects of solvent and the chirality of SWNTs on the loading of ssDNA oligomers more precisely, we accurately calculate the binding free energy of different type of nucleotide to zigzag SWNT (24,0) and armchair SWNT (14,14) by thermodynamic integration (TI) method. Fig. 7 shows the thermodynamic cycle employed to calculate the nucleotide-SWNT binding free energy, and Table 1 lists the nucleotide-SWNT binding free energy ΔF_{bind} for four combinations in this paper. ΔF_{ele}, ΔF_{vdw} are the electrostatic and vdW contributions to ΔF_{bind}, respectively. Herein, $\Delta F_{bind} = \Delta F_{ele} + \Delta F_{vdw}$. The obtained ΔF_{bind} of A-armchair (14,14) and T-armchair (24,0) is very close to the data of a recent paper.[43] Moreover, the order of binding strength between bases and SWNT is same as recent experimental and simulation works.[44,45] In CHARMM force field applied in this study, there is no special energy term for stacking interaction, therefore, the effect of π–π stacking have been integrate into the non-bonded vdW interaction. As table 1 shows, vdW interaction contributes most of the ΔF_{bind} (rang from 87.0% to 92.3%) of nucleotide-SWNT

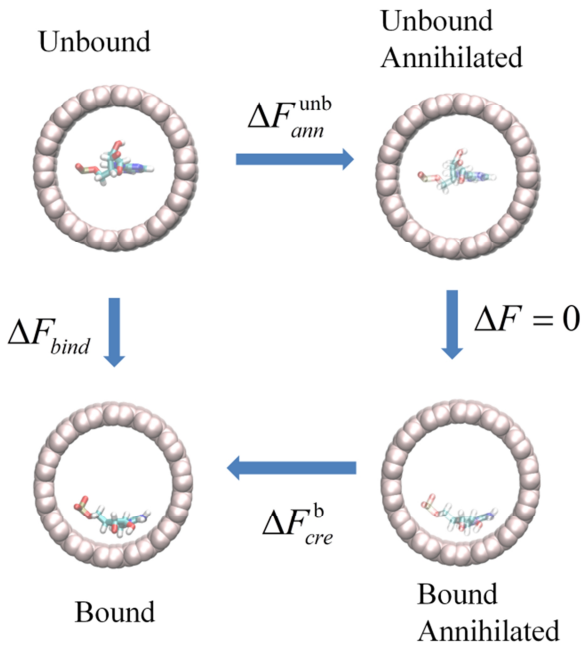

Fig. 7 The thermodynamic cycle employed to calculate the nucleotide-SWNT binding free energy. The binding free energy is defined as $\Delta F_{\text{bind}} = \Delta F_{\text{bound}} - \Delta F_{\text{unbound}}$. $\Delta F_{\text{cre}}^{\text{b}}$ and $\Delta F_{\text{ann}}^{\text{unb}}$ are the free energy required to create and annihilate nucleotide interactions in the bound and unbound states, respectively. With this scheme $\Delta F_{\text{bind}} = \Delta F_{\text{ann}}^{\text{unb}} + \Delta F_{\text{cre}}^{\text{b}}$. Annihilated nucleotides are partially transparent to present that they have no non-bonded interactions with themselves or the environment.

Table 1 Nucleotide-SWNT binding free energy ΔF_{bind} for four combinations in this study. ΔF_{ele}, ΔF_{vdw} are the electrostatic and vdW contributions to ΔF_{bind}, respectively. Here, $\Delta F_{\text{bind}} = \Delta F_{\text{ele}} + \Delta F_{\text{vdw}}$. All values in kJ/mol.

System	ΔF_{ele}	ΔF_{vdW}	ΔF_{bind}
A-zigzag SWNT (24,0)	-4.2±0.8	-35.1±1.3	-39.3±2.1
A-armchair SWNT (14,14)	-3.8±0.4	-31.4±0.8	-35.2±1.2
T-zigzag SWNT (24,0)	-5.0±0.8	-33.5±0.8	-38.5±1.6
T-armchair SWNT (14,14)	-2.5±0.4	-30.1±1.3	-32.6±1.7

for all systems. As the majority of the vdW interaction between nucleotides and SWNTs origins from the π–π stacking interaction, these data also show evidence of the significant roles of stacking interaction in the nucleotide-SWNTs interaction and ssDNA loading process. Moreover, it also implies that the electrostatic interaction between nucleotides and water contribute around 10% of the nucleotide-SWNT binding free energy ΔF_{bind}. On the other hand, these data clearly shows the binding preference of both adenine and thymine to zigzag SWNT (24,0). The ΔF_{bind} of A-zigzag SWNT (24,0) is 4.1 kJ/mol stronger than that of A-armchair SWNT (14,14), while ΔF_{bind} of T-zigzag SWNT (24,0) is 5.9 kJ/mol stronger than that of T-armchair SWNT (14,14). Moreover, solvation effect plays an important role in the difference of binding free energy, as displayed in Table 1. The binding strength characterized by the free energy is in the order A-zigzag SWNT (24,0) > T-zigzag SWNT (24,0) > A-armchair SWNT (14,14) > T-armchair SWNT (14,14), which is roughly opposite with the order of ssDNA oligomers loading time A8@SWNT(24,0) < T8@SWNT(24,0) ≈ A8@SWNT(14,14) < T8@SWNT(14,14) observed in classical MD. For ssDNA-SWNTs binding free energy, it is not additive with the binding free energy between its unit and wall, because the conformational entropy change of ssDNA as well as entropy change of water molecules repelled out of the SWNTs may also have certain effects on the interior adsorption of ssDNA. However, by accurate binding free energy calculation for nucleotide-SWNTs, we found that the binding free energy of nucleotide-SWNTs have certain correlation with the loading time of corresponding ssDNA into SWNTs. More specifically, with strongest binding free energy of A-zigzag SWNT (24,0), poly$(A)_8$ has the fastest loading into the cavity of SWNT (24,0), and vice versa.

4. Conclusion

In this study, different type of ssDNA oligomers including poly$(A)_8$ and poly$(T)_8$ were selected as a model to investigate the mechanism and dynamics of loading of ssDNA into SWNTs with different chirality by MD simulations. Our simulation results showed that the loading of different ssDNA oligomers into the zigzag SWNT is much easier than the armchair SWNT does. The order of ssDNA oligomers loading time is A8@SWNT (24,0) < T8@SWNT (24,0) ≈ A8@SWNT (14,14) < T8@SWNT (14,14) with specific starting configuration and position of ssDNA. Confined in both zigzag and armchair type SWNTs, ssDNA oligomers have helical structure to increase the contact area between their bases and wall, and their bases adapt the orientation that parallel to the interior wall. The order of the loading dynamics could also be validated by potential of mean force calculation through multiple SMD simulation of pulling ssDNA out of SWNT. Accurate free energy calculation reveals that the binding strength of nucleotide-SWNTs is in the order of A-zigzag SWNT (24,0) > T-zigzag SWNT (24,0) > A-armchair SWNT (14,14) > T-armchair SWNT (14,14), and it has correlation with the loading time of

corresponding ssDNA oligomers into SWNTs. These results indicate that the chirality of SWNTs has large effect on the binding strength of nucleotides, and hence affect the loading dynamics of ssDNA into SWNTs. The mechanism and dynamics of DNA loading into SWNTs revealed in this study could help us to better understand the DNA-CNTs interaction from the molecular level, and may have potential applications in the design of a biomimetic CNTs for drug and gene delivery system.

Acknowledgments

We gratefully acknowledge the financial support by the National Natural Science Foundation of China (Grant Nos. 21403049, 21273200), Zhejiang Provincial Natural Science Foundation of China (Grant Nos. LY14B030008 and LY14H300006) and start funding of Hangzhou Normal University (Nos. PE13002004041).

References

1. N. Pinna, *J. Mater. Chem.*, 2007, **17**, 2769-2774.
2. C. Sanchez, P. Belleville, M. Popall and L. Nicole, *Chem. Soc. Rev.*, 2011, **40**, 696-753.
3. S. J. Lee, S. S. Lee, M. S. Lah, J.-M. Hong and J. H. Jung, *Chem. Commun.*, 2006, 4539-4541.
4. S. Kango, S. Kalia, A. Celli, J. Njuguna, Y. Habibi and R. Kumar, *Prog. Polym. Sci.*, 2013, **38**, 1232-1261.
5. C. D. S. Brites, P. P. Lima, N. J. O. Silva, A. Millán, V. S. Amaral, F. Palacio and L. D. Carlos, *J. Lumin.*, 2013, **133**, 230-232.
6. S. Iijima and T. Ichihashi, *Nature*, 1993, **363**, 603-605.
7. M. M. J. Treacy, T. W. Ebbesen and J. M. Gibson, *Nature*, 1996, **381**, 678-680.
8. R. H. Baughman, A. A. Zakhidov and W. A. de Heer, *Science*, 2002, **297**, 787-792.
9. M. G. C. Kahn, S. Banerjee and S. S. Wong, *Nano Lett.*, 2002, **2**, 1215-1218.
10. J. Wang, M. Musameh and Y. Lin, *J. Am. Chem. Soc.*, 2003, **125**, 2408-2409.
11. K. Besteman, J.-O. Lee, F. G. M. Wiertz, H. A. Heering and C. Dekker, *Nano Lett.*, 2003, **3**, 727-730.
12. X. Tan, M. Li, P. Cai, L. Luo and X. Zou, *Anal. Biochem.*, 2005, **337**, 111-120.
13. Z. Liu, X. Sun, N. Nakayama-Ratchford and H. Dai, *ACS Nano*, 2007, **1**, 50-56.
14. R. P. Feazell, N. Nakayama-Ratchford, H. Dai and S. J. Lippard, *J. Am. Chem. Soc.*, 2007, **129**, 8438-8439.
15. R. Singh, D. Pantarotto, D. McCarthy, O. Chaloin, J. Hoebeke, C. D. Partidos, J.-P. Briand, M. Prato, A. Bianco and K. Kostarelos, *J. Am. Chem. Soc.*, 2005, **127**, 4388-4396.
16. K. S. Siu, X. Zheng, Y. Liu, Y. Zhang, X. Zhang, D. Chen, K. Yuan, E. R. Gillies, J. Koropatnick and W.-P. Min, *Bioconjugate Chem.*, 2014, **25**, 1744-1751.
17. J. Geng, K. Kim, J. Zhang, A. Escalada, R. Tunuguntla, L. R. Comolli, F. I. Allen, A. V. Shnyrova, K. R. Cho, D. Munoz, Y. M. Wang, C. P. Grigoropoulos, C. M. Ajo-Franklin, V. A. Frolov and A. Noy, *Nature*, 2014, **514**, 612-615.
18. M. Bottini, F. Cerignoli, M. I. Dawson, A. Magrini, N. Rosato and T. Mustelin, *Biomacromolecules*, 2006, **7**, 2259-2263.
19. E. Katz and I. Willner, *ChemPhysChem*, 2004, **5**, 1084-1104.
20. N. W. S. Kam and H. Dai, *J. Am. Chem. Soc.*, 2005, **127**, 6021-6026.
21. V. Lulevich, S. Kim, C. P. Grigoropoulos and A. Noy, *Nano Lett.*, 2011, **11**, 1171-1176.

22. H. Gao, Y. Kong, D. Cui and C. S. Ozkan, *Nano Lett.*, 2003, **3**, 471-473.
23. F. F. Contreras-Torres and E. Martínez-Lorán, *Wiley Interdisciplinary Reviews: Computational Molecular Science*, 2011, **1**, 902-919.
24. A. Clavier, S. Kraszewski, C. Ramseyer and F. Picaud, *J. Biotechnol.*, 2013, **164**, 13-18.
25. Y.-C. Liu, J.-W. Shen, K. Gubbins, J. Moore, T. Wu and Q. Wang, *Phys. Rev. B*, 2008, **77**, 125438.
26. R. Duggal and M. Pasquali, *Phys. Rev. Lett.*, 2006, **96**, 246104.
27. A. Kolesnikov, J.-M. Zanotti, C.-K. Loong, P. Thiyagarajan, A. Moravsky, R. Loutfy and C. Burnham, *Phys. Rev. Lett.*, 2004, **93**, 035503.
28. G. Hummer, J. C. Rasaiah and J. P. Noworyta, *Nature*, 2001, **414**, 188-190.
29. Y. Kang, Y.-C. Liu, Q. Wang, J.-W. Shen, T. Wu and W.-J. Guan, *Biomaterials*, 2009, **30**, 2807-2815.
30. Z.-S. Zhang, Y. Kang, L.-J. Liang, Y.-C. Liu, T. Wu and Q. Wang, *Biomaterials*, 2014, **35**, 1771-1778.
31. Y. Kang, Q. Wang, Y.-C. Liu, J.-W. Shen and T. Wu, *J. Phys. Chem. B*, 2010, **114**, 2869-2875.
32. J. C. Phillips, R. Braun, W. Wang, J. Gumbart, E. Tajkhorshid, E. Villa, C. Chipot, R. D. Skeel, L. Kalé and K. Schulten, *J. Comput. Chem.*, 2005, **26**, 1781-1802.
33. A. D. MacKerell, D. Bashford, M. Bellott, R. L. Dunbrack, J. D. Evanseck, M. J. Field, S. Fischer, J. Gao, H. Guo, S. Ha, D. Joseph-McCarthy, L. Kuchnir, K. Kuczera, F. T. K. Lau, C. Mattos, S. Michnick, T. Ngo, D. T. Nguyen, B. Prodhom, W. E. Reiher, B. Roux, M. Schlenkrich, J. C. Smith, R. Stote, J. Straub, M. Watanabe, J. Wiórkiewicz-Kuczera, D. Yin and M. Karplus, *J. Phys. Chem. B*, 1998, **102**, 3586-3616.
34. E. Neria, S. Fischer, M. Karplus, *J. Chem. Phys*. 1996, **105**, 1902-1921.
35. J. H. Walther, R. Jaffe, T. Halicioglu and P. Koumoutsakos, *J. Phys. Chem. B*, 2001, **105**, 9980-9987.
36. J.-W. Shen, T. Wu, Q. Wang and Y. Kang, *Biomaterials*, 2008, **29**, 3847-3855.
37. J.-W. Shen, T. Wu, Q. Wang, Y. Kang and X. Chen, *Chemphyschem*, 2009, **10**, 1260-1269.
38. T. Darden, D. York and L. Pedersen, *J. Chem. Phys.*, 1993, **98**, 10089-10092.
39. R. J. Radmer and P. A. Kollman, *J. Comput. Chem.*, 1997, **18**, 902-919.
40. Y. V. Shtogun, L. M. Woods and G. I. Dovbeshko, *J. Phys. Chem. C*, 2007, **111**, 18174-18181.

41. X. Fan, E. Dickey, P. Eklund, K. Williams, L. Grigorian, R. Buczko, S. Pantelides and S. Pennycook, *Phys. Rev. Lett.*, 2000, **84**, 4621-4624.

42. C. Janiak, *J. Chem. Soc., Dalton Trans.*, 2000, 3885-3896.

43. R. R. Johnson, A. T. C. Johnson and M. L. Klein, *Small*, 2010, **6**, 31-34.

44. F. Albertorio, M. E. Hughes, J. A. Golovchenko and D. Branton, *Nanotechnology*, 2009, **20**, 395101.

45. M. L. Mayo, Z. Q. Chen and S. V. Kilina, *J. Phys. Chem. Lett.*, 2012, **3**, 2790-2797.